

University of Nebraska - Lincoln

DigitalCommons@University of Nebraska - Lincoln

Faculty Publications in Food Science and
Technology

Food Science and Technology Department

6-2015

A prototype on-line AOTF hyperspectral image acquisition system for tenderness assessment of beef carcasses

Govindarajan Konda Naganathan
University of Nebraska-Lincoln

Kim Cluff
University of Nebraska-Lincoln, kcluff1@gmail.com


Ashok Samal
University of Nebraska-Lincoln, asamal1@unl.edu

Chris Calkins
University of Nebraska-Lincoln, ccalkins1@unl.edu

David D. Jones
University of Nebraska-Lincoln, david.jones@unl.edu

See next page for additional authors

Follow this and additional works at: <http://digitalcommons.unl.edu/foodsciefacpub>

 Part of the [Food Processing Commons](#), [Meat Science Commons](#), and the [Other Food Science Commons](#)

Konda Naganathan, Govindarajan; Cluff, Kim; Samal, Ashok; Calkins, Chris; Jones, David D.; Lorenzen, Carol; and Subbiah, Jeyamkondan, "A prototype on-line AOTF hyperspectral image acquisition system for tenderness assessment of beef carcasses" (2015). *Faculty Publications in Food Science and Technology*. 134.
<http://digitalcommons.unl.edu/foodsciefacpub/134>

This Article is brought to you for free and open access by the Food Science and Technology Department at DigitalCommons@University of Nebraska - Lincoln. It has been accepted for inclusion in Faculty Publications in Food Science and Technology by an authorized administrator of DigitalCommons@University of Nebraska - Lincoln.

Authors

Govindarajan Konda Naganathan, Kim Cluff, Ashok Samal, Chris Calkins, David D. Jones, Carol Lorenzen, and Jeyamkondan Subbiah

A prototype on-line AOTF hyperspectral image acquisition system for tenderness assessment of beef carcasses

Govindarajan Konda Naganathan,¹ Kim Cluff,¹ Ashok Samal,² Chris R. Calkins,³
David D. Jones,¹ Carol L. Lorenzen,⁴ and Jeyamkondan Subbiah^{1,5}

1. Biological Systems Engineering, University of Nebraska–Lincoln, Lincoln, NE 68583

2. Computer Science and Engineering, University of Nebraska–Lincoln, Lincoln, NE 68588

3. Animal Science, University of Nebraska–Lincoln, Lincoln, NE 68583-0908

4. Animal Science Research Center, University of Missouri, Columbia, MO 65211

5. Food Science and Technology, University of Nebraska–Lincoln, Lincoln, NE 68583,

Corresponding author — J. Subbiah, 212 L.W. Chase Hall, University of Nebraska–Lincoln, Lincoln, NE 68583-0726, USA;
tel 1 402 472-4944, fax 402 472-6338, email jeyam.subbiah@unl.edu

Abstract

A prototype on-line acousto-optic tunable filter (AOTF)-based hyperspectral image acquisition system ($\lambda = 450\text{--}900\text{ nm}$) was developed for tenderness assessment of beef carcasses. Hyperspectral images of ribeye muscle on stationary hanging beef carcasses ($n = 338$) at 2-day postmortem were acquired in commercial beef slaughter or packing plants. After image acquisition, a strip steak was cut from each carcass, vacuum packaged, aged for 14 days, cooked, and slice shear force tenderness scores were collected by an independent lab. Beef hyperspectral images were mosaicked together and principal component (PC) analysis was conducted to reduce the spectral dimension. Six different textural feature sets were extracted from the PC images and used in Fisher's linear discriminant model to classify beef samples into two tenderness categories: tender and tough. The pooled feature model performed better than the other models with a tender certification accuracy of 92.9% and 87.8% in cross-validation and third-party true validation, respectively. Two additional metrics namely overall accuracy and a custom defined metric called accuracy index, were used to compare the tenderness prediction models.

Keywords: Beef grading, Acousto-optic tunable filter, Discriminant model, Textural features, Feature selection, Principal component analysis

1. Introduction

The sustainability of the beef industry is of vital importance to U.S. agriculture. Guaranteeing a good eating experience is a top priority for the beef industry (Boleman et al., 1998; Brooks et al., 2000; Lorenzen et al., 1993; McKenna et al., 2002; Morgan et al., 1991). However, the beef industry has long struggled to produce consistently tender products. In order to manage and reduce variation in tenderness, one must be able to determine this trait effectively and accurately. The beef industry is therefore in need of an instrument to measure tenderness in a noninvasive manner.

Hyperspectral imaging (HSI) is a combination of video image analysis and near-infrared spectroscopy (NIR), which are the two most commonly used technologies for predicting beef tenderness (Konda Naganathan et al., 2008a, 2008b). Near-infrared spectroscopy works by measuring the relative intensity of light reflected from an object across a broad spectrum of wavelengths. Hyperspectral imaging provides greater detail by providing the same information on a pixel-by-pixel basis. This technique simultaneously

collects muscle structure and biochemical information that have high degrees of relationship with beef tenderness. The muscle structure and biochemical properties include muscle pH which influences activity of proteolytic enzymes, sarcomere length (an indication of degree of muscular contraction at rigor), extent of proteolysis, amount and insolubility of connective tissue (collagen), and composition (Felter, 2007). This concept was demonstrated using a bench-top HSI system (Konda Naganathan et al., 2008a, 2008b). A canonical discriminant model was developed using image textural features, and it forecasted two tenderness categories—namely tender and tough—with an accuracy of 94.5% (Konda Naganathan et al., 2008a). Several other studies (Cluff et al., 2008, 2013; ElMasry et al., 2012; Wu et al., 2012) have also shown the potential of hyperspectral imaging for beef tenderness assessment. A comprehensive review on the application of hyperspectral imaging for detecting quality attributes of red meat, including tenderness in beef, can be found elsewhere (Xiong et al., 2012).

Most of the HSI systems used for beef tenderness prediction are off-line systems that require a one-inch thick steak to be excised

from the carcass to predict tenderness. However, the beef industry does not want to excise one-inch ribeye steak from each carcass for tenderness prediction as it is very expensive and degrades the value of that primal cut. The industry wants an instrument that can image the ribeye exposed on a ribbed carcass on-line. Therefore, the first objective of this study was to develop a prototype on-line acousto-optic tunable filter (AOTF)-based HSI system for acquiring hyperspectral images of ribeye muscle on hanging beef carcasses in commercial beef packing plants. The AOTF HSI system can acquire hyperspectral images of the ribeye muscle without the need to move the ribeye muscle as in the case of dispersive HSI systems, such as spectrograph-based HSI systems. The AOTF HSI system can be converted to a multispectral imaging (MSI) system easily by programming it to acquire only select wavelength images for faster image acquisition and analysis.

The hyperspectral image analysis method contains the following steps: (1) image calibration, (2) region-of-interest (ROI) selection, (3) spectral dimensionality reduction, (4) image feature extraction, (5) image feature selection, and (6) tenderness prediction model development (Konda Naganathan, 2011; Subbiah et al., 2012, 2014). Of these steps, image feature extraction is an important step, as image textural features have been identified as potential indicators of beef tenderness (Li et al., 1999, 2001). Even though a number of textural feature extraction algorithms have been tested for beef tenderness prediction using RGB images (Jackman et al., 2008), only gray level co-occurrence matrix and wavelet features have been tested in the hyperspectral image domain for beef and pork tenderness evaluation (Barbin et al., 2013; Konda Naganathan et al., 2008a, 2008b). Therefore, the second objective of this study was to test various textural feature extraction algorithms for beef tenderness prediction.

Hundreds of textural features can be extracted from a hyperspectral image because it usually contains hundreds of tonal images, each representing a wavelength. When such a large number of features are used to predict one outcome, in this case tenderness, chances of developing an over-fitted tenderness prediction model are very high. An over-fitted model performs exceptionally well for a data set that was used to build the model. When this over fitted model is evaluated using a new data set, it fails drastically. One way to test whether or not a tenderness prediction model is over fitted is to implement true validation of the model using a new data set. So, the third objective of this study was to conduct a third-party validation to evaluate the accuracy of the hyperspectral imaging system.

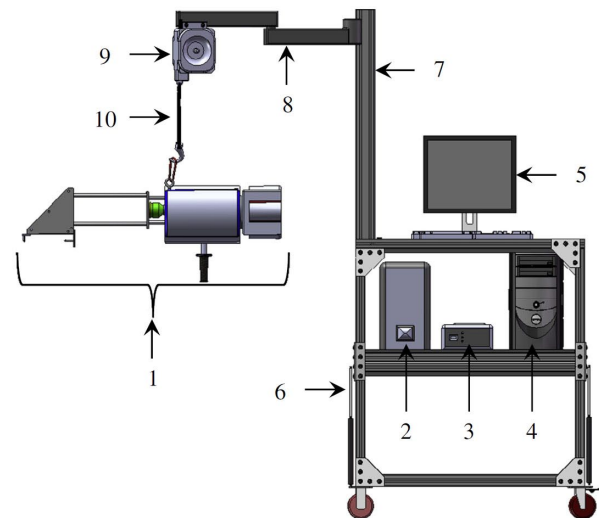
In summary, the objectives of this study were to:

- (1) develop a prototype on-line acousto-optic tunable filter (AOTF)-based hyperspectral imaging system for acquiring images of the ribeye muscle on hanging beef carcasses in commercial beef packing plants,
- (2) develop methods to predict beef tenderness from hyperspectral images; in particular, compare different textural feature extraction algorithms for their usefulness in beef tenderness assessment, and
- (3) conduct a third-party true validation of the AOTF system for beef tenderness prediction.

2. Materials and methods

2.1. Prototype on-line hyperspectral image acquisition system

A prototype on-line AOTF HSI system (Figure 1) was designed and fabricated to collect reflectance images of ribeye muscle (*longissimus dorsi*) on hanging beef carcasses in commercial beef packing plants. The system consisted of a camera module, a radio frequency (RF) unit (Model: 150-10DFS-16X1, ChromoDynamics,



[a]. Entire system

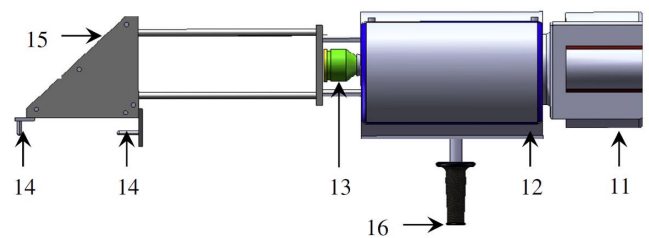


Figure 1. Schematic of the prototype on-line acousto-optic tunable filter (AOTF)-based hyperspectral imaging system (HSI). Parts: (1) camera module, (2) radio frequency unit, (3) uninterruptible power supply, (4) computer, (5) monitor, (6) height-adjustable mobile console, (7) vertical tower, (8) cantilever, (9) tool balancer, (10) tension-adjustable retractable cable, (11) camera, (12) acousto-optic tunable filter, (13) lens, (14) locating plates, (15) periscope assembly that houses a mirror and light bulbs, and (16) handle.

Lakewood, NJ), and a computer (Acer Aspire T135 equipped with a 2.6 GHz AMD dual core processor, and 2 GB of RAM), and mounted on an adjustable-height mobile console.

2.1.1. Camera module

The camera module included an Andor iXON camera (Model: DU-885k-CSO-#VP, Andor, South Windsor, CT.), an AOTF optical head (Model: HSi-300, ChromoDynamics, Lakewood, NJ), a lens (Model: 24 mm f/2.8D AF, Nikon Inc., Melville, NY), and a custom-built periscope assembly. The AOTF optical head had a spectral sensitivity in the visible-near infrared (VNIR) region ranging from 450 to 900 nm and had a spectral resolution of 2 nm at 600 nm and 4.2 nm at 900 nm. In the AOTF HSI system, spectral resolution is a function of wavelength. Therefore, the system had different spectral resolutions at different wavelengths. The Andor iXON camera is an ultrasensitive high performance scientific camera with a 2D EMCCD sensor array with a resolution of 1004×1002 pixels. However, a smaller rectangular field of view was sufficient to completely cover beef ribeye muscle. Therefore, an image size of 600×1000 pixels was found sufficient to capture the entire beef ribeye muscle; so, the rest of the pixels were cropped out during image acquisition to reduce the image data size. Additionally, the Andor camera had a frame rate of 31.4 frames per second with a quantum efficiency of 65% at 600 nm. The Nikon lens had a focal length of 24 mm and a maximum aperture of 2.8. The RF unit sent a radio frequency electronic signal

to the AOTF optical head and based on the frequency of the signal, the AOTF optical head controlled which wavelengths of light were allowed to the camera.

2.1.2. Periscope assembly

In beef packing plants, the ribeye muscle is exposed by making a cut between the 12th and 13th rib of each beef carcass. The ribbing process separates the hind and fore quarters of a beef carcass with a gap 20–25 cm at the dorsal end. To accommodate this size limitation, a periscope-type design was used in building the system. The periscope assembly was a part of the camera module and comprised of a mirror, two tungsten halogen bulbs (Model: EZK 12 V, 150 W, Philips), and locating plates. A periscope design was employed so that the system would not be obstructed by the hindquarter of the carcass, which is directly above the exposed ribeye. A mirror was positioned at a 45° angle, so that the reflected signal from the beef ribeye would be directed at a 90° angle onto the AOTF optical head. The distance of the mirror from the lens was optimized and fixed to cover a field of view (FOV) of size 13 cm × 18 cm that would cover the entire ribeye muscle. In order to provide uniform lighting, diffusers were placed in front of the bulbs. The purpose of the locating plates was to firmly and positively hold the camera module onto the exposed portion of the carcass during image acquisition.

2.1.3. Mobile console

The computer, the RF unit, and an uninterrupted power supply (UPS) unit were placed in the console (Figure 1). It was also equipped with a vertical tower, a cantilever, and a tool balancer. One end of the cantilever was attached to the vertical tower and the other end was equipped with a tool balancer. This tool balancer had a retractable, tension-adjustable cable and provided the facility to operate at a preset height. The camera module was connected to the tool balancer cable through a snap-style clip. The tool balancer bore the weight of the camera module and provided ease of handling. It also placed the camera module at approximately the same height as the exposed ribeye on a hanging carcass. The cantilever provided the ability to image carcasses on two adjacent rails without moving the mobile console, while stationing the mobile console between the two rails. In addition, the console was equipped with gas springs at its bottom to adjust its height. During transport, the console was lowered, but during operation, it was kept in a raised position. In summary, this design allowed portability, moving the system from plant to plant, and mobility within the plant. The system power was backed up with an UPS unit to safeguard the system from power surge and failure.

2.2. Samples

Data were collected in two regional beef packing plants over a period of three days. A total of 338 beef carcasses were imaged after 36–48 h of postmortem. In order to have tenderness variation in the sample population, beef carcasses representing the USDA quality grades of Prime, Choice, Select, and Standard were used. The USDA quality grades were assigned by a trained USDA grader following the USDA beef carcass grading standards (USDA, 1997). The selected carcasses were railed off for image acquisition.

2.3. Hyperspectral image acquisition

Figure 2 demonstrates how the prototype on-line AOTF HSI system was used to acquire an image of the ribeye muscle on a hanging beef carcass in a commercial beef packing plant. An integration time of 35 ms, a gain factor of 2, and a band interval of 5 nm were used as imaging parameters. This setup provided 91 bands between 450 nm and 900 nm. The camera module of the system



Figure 2. Acquiring image of beef ribeye using the prototype on-line acousto-optic tunable filter (AOTF)-based hyperspectral imaging system (HSI).

was placed on the exposed ribeye muscle so that the camera covered the entire *longissimus dorsi* muscle. The camera module was moved laterally in such a way that the locating plates came in firm contact with the hanging carcass and provided a steady setup to avoid shaking of the camera module during image acquisition. After the firm placement, the camera was triggered to acquire a hyperspectral image. It took approximately four seconds to acquire one hyperspectral image of the beef ribeye muscle.

In addition to the beef images, dark and white reference images were acquired at approximately 45–60 min intervals. The reference images were used to calibrate the beef images. The white images were collected using a 99% spectralon plate (Labsphere, North Sutton, NH), whereas the dark images were collected by closing the camera lens with a cap. The size of the spectralon plate was 13 cm × 13 cm, which did not cover the entire imaging FOV. Therefore, two white reference images, one covering the bottom half of the FOV and the other covering the top half of the FOV, were acquired. The two white reference images were merged by averaging the overlapping regions and a combined white reference image size 13 cm × 18 cm was created.

2.4. Reference tenderness scores and carcass traits

Carcass characteristics such as marbling, ribeye area, and the USDA quality and yield grades were collected. The carcass characteristics were estimated by a USDA meat grader following the USDA grading protocols (USDA, 1997). After imaging the ribeye of the hanging beef carcasses, strip loin steaks were cut from the carcasses and vacuum packaged. All strip loin steaks were aged for 14 days in refrigerated conditions (not frozen) at 2 °C by following a standard protocol (AMSA, 1995). Immediately after the aging period, the steaks were cooked and slice shear force (SSF) values were collected by an independent third-party lab following the procedures explained by Shackelford et al. (1999). The samples having SSF values greater than 245.2 N (Lorenzen et al., 2009) were considered as tough and the rest were classified as tender. Within each day of sample collection, the samples were sorted based on the SSF values and the carcasses were alternately assigned for training and validation to ensure that the tenderness distribution within each data set was similar. The SSF values pertaining to the training set were shared with the system provider for developing tenderness calibration equations. The SSF values pertaining to the validation dataset were sequestered and the third-party lab kept it

with themselves for validating the tenderness predictions assigned by the system.

2.5. Hyperspectral image processing

Image calibration and processing algorithms were conducted in the lab using ENVI 4.8 (ITTVIS, Boulder, CO), and MATLAB 7.1 (The MathWorks Inc., Natick, MA) with Image Processing, Wavelet, and Statistics Toolboxes. A flowchart showing the different steps of image processing is shown in Figure 3.

2.5.1. Image calibration and region-of-interest (ROI) selection

Calibrated beef reflectance images were obtained by subtracting the dark image and dividing with the dark-subtracted white image (Figure 3). Even after calibrating the beef images, some bright spots at the middle of the image and dark spots at the top and bottom portions of the image remained due to uneven illumination. Lighting variation was more predominant in the vertical dimension as compared to the horizontal dimension of the image. Therefore, the cross-track illumination correction function (ENVI, 2014) available in ENVI was used to reduce the lighting variations along the vertical dimension of the image. The effects of uneven illumination were minimized, after implementing the illumination correction. After calibration, a region-of-interest (ROI) of size 180×400 pixels (28.8×64 mm) was manually selected within the ribeye muscle area. All subsequent image processing steps were performed on these ROI hyperspectral images.

2.5.2. Mosaic principal component analysis

Hyperspectral images are collected at very narrow wavelength intervals that result in redundant (or correlated) information in adjacent (wavelength) images. One of the methods to reduce the dimensionality of a hyperspectral image is principal component analysis (PCA). PCA determines principal component (PC) images, such that they explain maximum variation of the original hyperspectral image. In mosaic PCA, all the hyperspectral images of the training set were mosaicked (assembling images next to each other in a systematic manner, similar to an image montage) together and the resulting mosaicked image was subjected to the PCA procedure, and loading vectors were obtained (Konda Naganathan, 2011; Subbiah et al., 2014). This method explains both within-sample and between-sample variations (Konda Naganathan, 2011; Subbiah et al., 2014). The first three principal components (PC) explained over 99% of the variation of the original image. Therefore, three PC images (Figure 4) were created for each hyperspectral image by multiplying the first three loading vectors with the hyperspectral images. Additional analyses were performed on the PC band images.

2.5.3. Feature extraction

One of the objectives of this study was to extract different hyperspectral image feature sets and compare their relative performances in predicting beef tenderness. Even though some of these feature sets have been evaluated already in the RGB image domain for beef tenderness, only a few feature sets such as gray level co-occurrence matrix features and wavelet features, have been evaluated in the hyperspectral image domain especially for beef and pork tenderness prediction (Barbin et al., 2013; Konda Naganathan et al., 2008a and Konda Naganathan et al., 2008b). Therefore, six different sets of features were obtained from the hyperspectral images: (1) descriptive statistical features (DSF), (2) wavelet features (WF), (3) gray level co-occurrence matrix features (GLCMF), (4) Gabor features (GF), (5) Laws features (LF), and (6) local binary pattern features (LBP). An additional analysis scenario, pooled features (PF), was also created by pooling all the features. These features sets provided a diverse set of features. The wavelet and

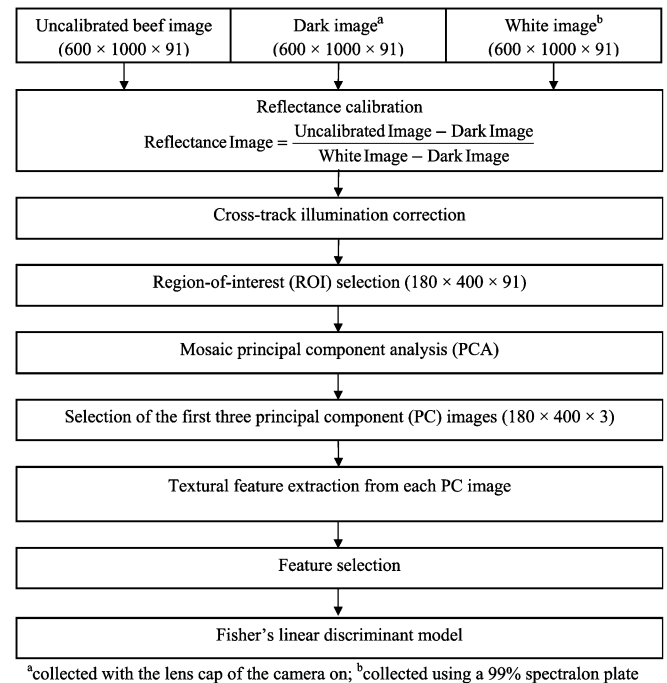


Figure 3. Flow chart showing different image processing steps.

Gabor features are joint spatial-frequency features, whereas the other features are spatial features. The PC images were processed by the feature extraction algorithms written in MATLAB (The MathWorks Inc., Natick, MA).

2.5.3.1. Descriptive statistical features (DSF) — Six descriptive statistical features: mean, standard deviation, second moment, entropy, skewness and kurtosis, were extracted from each PC image. A total of 18 descriptive statistical features (3 PC images \times 6 descriptive features per PC image) were extracted. These features explained some of the following image attributes: average gray-level value, dispersion of the gray-level values, uniformity, information content, symmetry or asymmetry, and distribution.

2.5.3.2. Wavelet features (WF) — In this analysis, symmetric Daubechies 4 wavelet was used as the mother wavelet because it was shown to perform better than the other mother wavelets for predicting beef palatability (Jackman et al., 2009). Four decomposition levels were used. At each decomposition level, the input PC image was decomposed into one low frequency approximation image and three high frequency detail images, one in each orientation – horizontal, vertical and diagonal. The detail images were averaged to get rotationally invariant results (Subbiah, 2004). The approximation image became the input image for the next level of decomposition. For each PC image, five features namely four energy features (Subbiah, 2004) from the Level-1 to Level-4 detail images and one energy feature from the Level-4 approximation image, were computed. A total of 15 wavelet features were extracted (3 PC images \times 5 descriptive features per PC image).

2.5.3.3. Gray-level co-occurrence matrix features (GLCMF) — On the PC images, gray-level co-occurrence matrix (GLCM) analysis with $g = 256$, $d = 1$ and $\theta = \{0^\circ, 45^\circ, 90^\circ, 135^\circ\}$ was conducted for extracting image texture features (Konda Naganathan et al., 2008a and Li et al., 1999). The GLCM procedure produced four textural features: contrast, correlation, entropy and homogeneity, for each PC image. A total of 12 GLCM features were extracted (3 PC images \times 4 GLCM features per PC image).

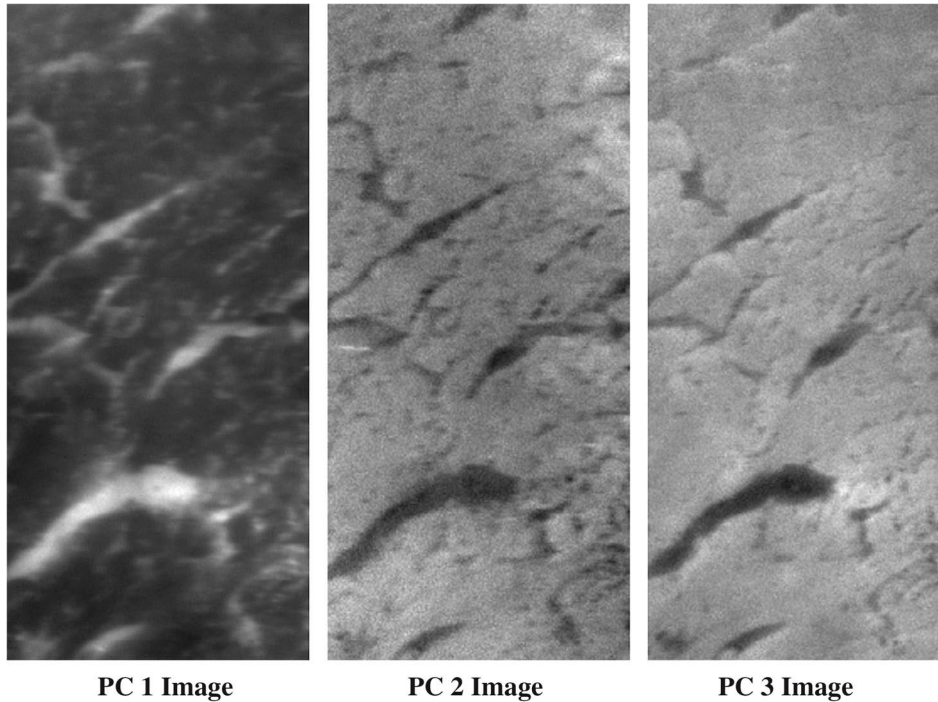


Figure 4. First three principal component (PC) images.

2.5.3.4. Gabor features (GF) — The algorithm for the Gabor filter described in Manjunath and Ma (1996) was implemented. Gabor filter design requires four parameters: number of scales (S), number of orientations (K), center frequencies along the horizontal axis (U_h), and vertical axis (U_v). Gabor energy was calculated by using the parameters: $S = 4$, $K = 6$, $U_h = 0.05$, and $U_v = 0.4$ for the Gabor filter (Subbiah, 2004). Images from all orientations were averaged to obtain rotation invariant results. For each PC image, four energy values from the scale images were computed. A total of 12 Gabor features were extracted (3 PC images \times 4 Gabor features per PC image).

2.5.3.5. Laws features (LF) — The algorithm developed by Laws (1980) was used to compute these features. This algorithm determines image texture by evaluating average gray level (L), edges (E), spots (S), ripples (R), and waves (W) in an image. These measures are derived from five simple vectors: $L5 = [1, 4, 6, 4, 1]$, $E5 = [-1, -2, 0, 2, 1]$, $S5 = [-1, 0, 2, 0, -1]$, $R5 = [1, -4, 6, -4, 1]$ and $W5 = [-1, 2, 0, -2, -1]$. Mutual multiplication of these vectors results in 25 matrices, each of size 5×5 , known as Laws masks. These masks form 10 pairs of transposed masks such as E5L5 mask and L5E5 mask. The PC images were convolved with each of the 25 Laws masks, and 25 different Laws or intermediate images were created. Because of the non-zero mean characteristic, the L5L5 image was used to normalize the other 24 images. Also, the 10 transposed image pairs were added together to get 10 rotation invariant images. The other 4 images were multiplied by 2 to have the same scale as the rotation invariant images. For each PC image, this analysis produced 14 different Laws images and energy values of these images were computed. A total of 42 Laws features were extracted (3 PC images \times 14 Laws features per PC image).

2.5.3.6. Local binary pattern features (LBPF) — The algorithm described in Ojala et al. (1996) was used to extract local binary pattern features. These features are considered robust because they are not affected drastically by image variations caused by non-uniform illumination, rotation, scaling, and viewing angle (Ojala

et al., 1996). Three different neighborhood configurations, characterized by three different radii (1, 2, and 3 pixels) and 8 sampling points, were used. Two intermediate images namely LBP image and contrast image, were created. First a binary code image was created by thresholding the neighborhood by the gray value of its center. Then the binary code image was multiplied by a standard weight image to create an LBP code image. The gray level value of the center pixel in the LBP image was obtained by summing up the LBP code image. Similarly, the contrast image values were computed by subtracting the average of the gray levels below the center pixel from that of the gray levels above (or equal to) the center pixel. For each PC image, three LBP images and three contrast images, one for each radius, and six descriptive statistical features were computed from each LBP and contrast images. A total of 108 LBP features were extracted (3 PC images \times 6 intermediate images per PC image \times 6 LBP features per intermediate image).

2.6. Feature selection and fisher's linear discriminant (FLD) models

Using each of the feature sets mentioned above, seven different Fisher's linear discriminant (FLD) models were developed (Johnson, 1998). In addition to these image features, marbling was also considered as one of the features as it is shown to have a relationship with tenderness (Jeremiah, 1996). Prior to FLD modeling, a stepwise feature selection (STEPDISC procedure in SAS) was followed to identify image features that have the most tenderness discrimination power. A p -value of 0.15 was used to test the significance level of a feature during both forward addition and backward elimination. The developed FLD models were evaluated using leave-one-out cross-validation and third-party true validation.

2.7. Evaluation metrics

Overall accuracy (Equation (1)) is a traditional metric commonly used to evaluate classification models. Even though it is useful in other classification problems, it may not adequately explain the performance or usefulness of a beef tenderness prediction model

in imbalanced dataset such as the one collected in this study (more than 80% of the samples were tender in this study). Therefore, a 2×2 confusion matrix was first generated based on the actual and predicted tenderness classes or categories – tender and tough, and then four different accuracy values namely tender identification accuracy, tough identification accuracy, tender certification accuracy, and tough certification accuracy (Equations (2–5)), were computed. Of these accuracy measures, the tender certification accuracy is the most useful measure for the beef industry for making tenderness marketing claims. The tough identification accuracy is also equally important because any misclassification tough samples as tender affects the tenderness marketing claim. Therefore, a new metric called accuracy index (Equation (6)) was developed by weighting the tender certification accuracy and tough identification accuracy more (twice) than the other two accuracy measures. For comparing the tenderness prediction models, the tender certification accuracy, overall accuracy, and accuracy index values were used.

Overall Accuracy (OA)

$$= \frac{\text{Number of correctly predicted tender and tough samples}}{\text{Total number samples}} \quad (1)$$

Tender Certification Accuracy (TECA)

$$= \frac{\text{Number of correctly predicted tender samples}}{\text{Total number of predicted tender samples}} \quad (2)$$

Tough Identification Accuracy (TOIA)

$$= \frac{\text{Number of correctly predicted tough samples}}{\text{Total number of true tough samples}} \quad (3)$$

Tough Certification Accuracy (TOCA)

$$= \frac{\text{Number of correctly predicted tough samples}}{\text{Total number of predicted tough samples}} \quad (4)$$

Tender Identification Accuracy (TEIA)

$$= \frac{\text{Number of correctly predicted tender samples}}{\text{Total number of tender samples}} \quad (5)$$

Accuracy Index (AI)

$$= 1/6 [TEIA + 2 \times TOIA + 2 \times TECA + TOCA] \times 100 \quad (6)$$

3. Results and discussions

3.1. Adaptability

The prototype on-line system successfully acquired images of the ribeye muscle on hanging beef carcasses in multiple commercial beef packing plants. The periscope assembly of the system fit well within the ribbed opening of beef carcasses (Figure 2). In this respect, the system did not demand any change in the existing production practices for image acquisition. In addition, the time required to acquire a hyperspectral image of the ribeye muscle was four seconds, which is below the current rail speed (4–7 s) of a beef production facility. However, image acquisition was performed on stationary beef carcasses. In an ideal embodiment, image acquisition needs to be performed on carcasses moving on rails with a lighter and compact system.

3.2. Samples

Of the 338 samples, there were 277 tender samples (82%) and 61 tough samples (18%). Within the training set of 164 samples, 133 samples (81.1%) were in the tender category and the remaining 31 samples (18.9%) were in the tough category. Similarly, of the 174 samples in the validation set, 144 samples (82.8%) were in the tender category and the remaining 30 samples (17.2%) were in the tough category.

A histogram showing the distribution of SSF values or tenderness of the beef samples is provided in Figure 5. In addition, Table 1 presents the SSF or tenderness distribution of samples sequestered based on the USDA quality grades. The USDA Choice and Select samples represented 45.7% and 48.8%, respectively, of the total sample population and together they occupied 94.5% of the sample population. This distribution closely matched the one reported in the National Beef Quality Audit (McKenna et al., 2002). The percentage of the tough samples in the USDA Choice and Select category were 10.7% and 26.3%, respectively. George et al. (1999) reported the odds of obtaining a slightly tough or tougher rating for supermarket beef was 20–25% for USDA Choice and Select-grade strip steaks, respectively. For the data collected in this study, the odds of obtaining tough beef remained almost the same in the USDA Select grade, and were reduced by half in the USDA Choice grade. The USDA Select grade samples had higher SSF values compared to that of Choice grade.

3.3. Performance of the tenderness prediction models

The tenderness prediction results including the number of correctly predicted samples, number of misclassified samples, and evaluation metrics, for the various models are presented in Table 2. The pooled feature model had the highest tender certification accuracy, overall accuracy, and accuracy index value in both the cross-validation and third-party true validation. In cross-validation, the pooled feature model predicted a total of 112 samples as tender and out of these samples, 104 samples were true tender based on the measured SSF values. Similarly, 115 of the 131 predicted tender samples were true tender in third-party true validation. In other words, when the pooled feature model predicted a sample as tender, it was in fact tender for 92.9% and 87.8% accurate as per cross-validation and third-party true validation, respectively. The overall accuracy of the pooled feature model was 77.4% and 74.1% in cross-validation and third-party true validation, respectively. In cross-validation, it correctly identified 104 of the 133 true tender samples and 23 of the 31 true tough samples. In the third-party true validation, it correctly identified 115 of the 144 true tender samples and 14 of 30 the true tough samples.

In a study funded by the National Cattlemen's Beef Association (NCBA), Lorenzen et al. (2009) evaluated tenderness prediction instruments including the BeefCam and a spectroscopic system. For comparing the results of the NCBA study with that of this study, the accuracy index values of the BeefCam and spectroscopic systems were computed using the Equation (6) described earlier. In third-party true validation, the Beefcam and spectroscopy systems yielded accuracy index values of 53.9% and 58.3%, respectively. The accuracy index of the prototype on-line hyperspectral imaging system presented in this study was 76.1% in cross-validation and 63.6% in third-party true validation based on the pooled feature model.

The Laws feature model followed by the wavelet feature model predicted tenderness accurately next to the pooled feature model. The other models also had comparable accuracy metrics. Only a modest improvement in AI value was obtained when using pooled features because the image features had a good correlation within and between feature sets. Also, pooling the features increased the

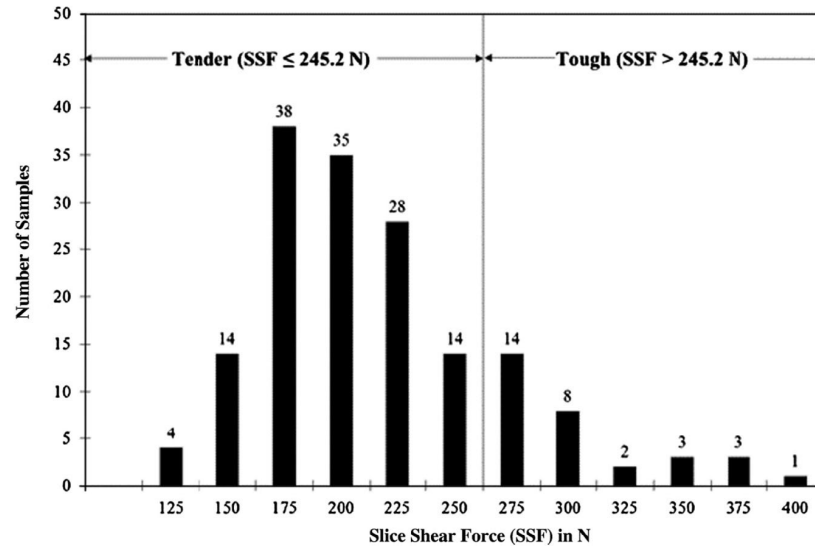


Figure 5. Distribution of the slice shear force (SSF) values or tenderness of the beef samples.

ratio of number of features to samples, which may have affected the performance of the feature selection algorithm.

The number of features used to build tenderness models ranged from three to eight. For example, the pooled feature model used a total of eight features – seven image features and marbling – in the tenderness classification equation. The seven image features included one descriptive statistical feature, one wavelet feature, three

Laws features and two local binary pattern features. Also, three of the seven features were computed from PC1 images, whereas the remaining four image features were computed from the PC3 images. These feature values were slightly higher for tender samples compared to those of tough samples. The performances of these models in cross-validation and third-party true validation were similar, which confirmed that the models were robust and not over

Table 1. Distribution of the measured slice shear force values or tenderness based on the USDA quality grade.

USDA quality grade	No. of samples	No. of true tender ^a samples	No. of true tough ^b samples	Slice shear force (N)				
				Minimum	Maximum	Mean	Median	Standard deviation
Choice	75	67	8	118.7	350.1	193.4	184.4	42.4
Select	80	59	21	117.7	393.2	213.6	206.9	58.0
Standard	9	7	2	108.9	338.3	204.9	185.3	76.5
Total	164	133	31	108.9	393.2	203.9	191.2	53.2

a. Slice shear force (SSF) \leq 245.2 N ; b. Slice shear force (SSF) $>$ 245.2 N.

Table 2. Comparison of beef tenderness prediction models developed using different hyperspectral image feature sets.

Models	Feature set	No. of features	Classification table				TECA	OA	AI
			True tender predicted as tender	True tender predicted as tough	True tough predicted as tender	True tough predicted as tough			
<i>Leave-one-out cross-validation</i>									
Model 1	DSF	7	99	34	12	19	89.2	72.0	68.5
Model 2	WF	4	90	43	10	21	90.0	67.7	69.3
Model 3	GLCMF	3	95	38	10	21	90.5	70.7	70.6
Model 4	GF	5	98	35	13	18	88.3	70.7	66.7
Model 5	LF	6	100	33	10	21	90.9	73.8	71.9
Model 6	LBPF	7	96	37	11	20	89.7	70.7	69.3
Model 7	PF	8	104	29	8	23	92.9	77.4	76.1
<i>Third-party true validation</i>									
Model 1	DSF	7	109	35	21	9	83.8	67.8	54.0
Model 2	WF	4	95	49	15	15	86.4	63.2	60.4
Model 3	GLCMF	3	92	52	21	9	81.4	58.0	50.2
Model 4	GF	5	99	45	17	13	85.3	64.4	58.1
Model 5	LF	6	108	36	17	13	86.4	69.5	60.2
Model 6	LBPF	7	103	41	19	11	84.4	65.5	55.8
Model 7	PF	8	115	29	16	14	87.8	74.1	63.6

DSF – Descriptive statistical features; WF – Wavelet features; GLCMF – Gray level co-occurrence matrix features; GF – Gabor features; LF – Laws features; LBPF – Local binary pattern features; PF – Pooled features; TECA – Tender certification accuracy (Equation (2)); OA – Overall accuracy (Equation (1)); AI – Accuracy index (Equation (6)).

fitted. The feature selection algorithm identified a compact set of stable and useful features. Given the number of features used in the prediction models and model performance, it was clear that the models were compact and robust.

3.4. Future work

Assigning a tenderness classification for a carcass using the AOTF HSI system is a two-step process: image acquisition and image analysis. A real-time system should implement both processes on-line, and should be completed within 4–7 s. As mentioned earlier, our system acquired images on-line within 4 s and processed them off-line in about three minutes, to assign a tenderness classification for a carcass. To make the AOTF HSI system for real-time beef tenderness assessment, the image processing time needs to be reduced and implemented on-line.

Each hyperspectral image collected by our system had 91 wavelength bands separated at 5 nm wavelength intervals. At this narrow interval, the bands tend to have redundant information. One way of not collecting redundant information is to collect images at a few key wavelengths only. This type of approach is called multispectral imaging (Subbiah et al., 2012, 2014). Fewer wavelength bands mean smaller data size, and faster processing. Also, it eliminates the dimensionality reduction step. With fewer bands in multispectral images, a considerably smaller number of features can be extracted in comparison to hyperspectral images. Therefore, the multivariate models developed using multispectral image features may be more robust. The concept of multispectral imaging not only reduces the time required to process the images, but also reduces the image acquisition time (Subbiah et al., 2014). A multispectral system cannot be developed without first identifying the key wavelengths. The algorithms used to analyze hyperspectral images may provide a way to determine key wavelengths. An advantage of the AOTF HSI system is that it can be programmed to acquire images of key wavelengths only. In this respect, the same system can be used as a multispectral system without any changes.

In addition, the following system improvements are recommended: (1) use a stable DC power source for illumination to counter the power fluctuations, (2) use a larger white reference plate that covers the entire field of view, and (3) add software functionality to detect image artifacts such as image blurring during acquisition.

4. Conclusions

This study has demonstrated that hyperspectral images of the ribeye muscle on hanging beef carcasses could be acquired in commercial beef slaughter or packing plants. It has also been demonstrated that the hyperspectral beef images acquired at 2-day postmortem could reliably predict 14-day aged, cooked beef tenderness. A novel prototype on-line acousto-optic tunable filter (AOTF) based hyperspectral image acquisition system was designed, developed, and used to acquire 338 ribeye hyperspectral images in two different regional beef slaughter or packing plants. On an average, this prototype on-line system needed 4 s to capture a hyperspectral image of a ribeye. Hyperspectral image features were extracted using six different feature extraction algorithms and modeled with Fisher's linear discriminant model to classify beef samples into two tenderness categories, tender and tough. The pooled feature model performed better than the other models with an overall accuracy of 77.4% and 74.1% in cross-validation and third-party true validation, respectively. The corresponding tender certification accuracies for the pooled feature model were higher (92.9% in cross-validation and 87.8% in third-party true validation), which is more useful for the beef industry to

make tenderness marketing claims. The other models particularly the Laws and wavelet feature models, also had comparable accuracy measures. Only a modest improvement in model performance was achieved when combining feature sets because the image features had a good correlation within and between feature sets. Future work is needed to demonstrate image acquisition on moving carcasses and integrate the image analysis and tenderness prediction equation with the image acquisition software. The prospect of converting this prototype on-line system to a commercial real-time system is high. This work will lead to labeling of accurate quality factors on beef products, which will add value to the products.

Acknowledgments — The authors would like to appreciate National Cattlemen's Beef Association and Nebraska Agricultural Experiment Station for providing funding for conducting this study. The authors are also thankful to the beef industry for providing access to the plant and the third-party lab for the slice shear force measurements of the beef samples.

References

- AMSA, 1995. Research Guidelines for Cookery, Sensory Evaluation and Instrumental Tenderness Measurements of Fresh Meat. American Meat Science Association and National Livestock and Meat Board, Chicago, IL.
- Barbin, D.F., Valous, N.A., Sun, D., 2013. Tenderness prediction in porcine longissimus dorsi muscles using instrumental measurements along with NIR hyperspectral and computer vision imagery. *Innovative Food Sci. Emerging Technol.* 20, 335–342.
- Boleman, S.L., Boleman, S.J., Morgan, W.W., Hale, D.S., Griffin, D.B., Savell, J.W., Ames, R.P., Smith, M.T., Tatum, J.D., Field, T.G., Smith, G.C., Gardner, B.A., Morgan, J.B., Northcutt, S.L., Dolezal, H.G., Gill, D.R., Ray, F.K., 1998. National Beef Quality Audit-1995: survey of producer-related defects and carcass quality and quantity attributes. *J. Anim. Sci.* 76 (1), 96–103.
- Brooks, J.C., Belew, J.B., Griffin, D.B., Gwartney, B.L., Hale, D.S., Henning, W.R., Johnson, D.D., Morgan, J.B., Parrish, F.C., Reagan, J.O., Savell, J.W., 2000. National beef tenderness survey-1998. *J. Anim. Sci.* 78 (7), 1852–1860.
- Cluff, K., Konda Naganathan, G., Subbiah, J., Lu, R., Calkins, C.R., Samal, A., 2008. Optical scattering in beef steak to predict tenderness using imaging spectroscopy in the VIS-NIR region. *Sens. Instrum. Food Qual. Saf.* 2 (3), 189–196.
- Cluff, K., Konda Naganathan, G., Subbiah, J., Samal, A., Calkins, C.R., 2013. Optical scattering with hyperspectral imaging to classify longissimus dorsi muscle based on beef tenderness using multivariate modeling. *Meat Sci.* 95 (1), 42–50.
- ElMasry, G., Sun, D., Allen, P., 2012. Near-infrared hyperspectral imaging for predicting colour, pH and tenderness of fresh beef. *J. Food Eng.* 110 (1), 127–140.
- ENVI, 2014. ENVI Documentation: Radiometric Correction Tools: <http://www.exelisvis.com/docs/OtherRadiometricCorrectionTools.html> (accessed October 15, 2014).
- Felter, L.M., 2007. Predicting Aged Beef Tenderness with Hyperspectral Imaging and the Relationship to Muscle Properties. Master's thesis. Animal Science, University of Nebraska-Lincoln.
- George, M.H., Tatum, J.D., Belk, K.E., Smith, G.C., 1999. An audit of retail beef loin steak tenderness conducted in eight U.S. cities. *J. Anim. Sci.* 77, 1735–1741.

- Jackman, P., Sun, D., Du, C., Allen, P., Downey, G., 2008. Prediction of beef eating quality from colour, marbling and wavelet texture features. *Meat Sci.* 80 (4), 1273–1281.
- Jackman, P., Sun, D., Allen, P., 2009. Comparison of various wavelet texture features to predict beef palatability. *Meat Sci.* 83 (1), 82–87.
- Jeremiah, L.E., 1996. The influence of subcutaneous fat thickness and marbling on beef: palatability and consumer acceptability. *Food Res. Int.* 29 (5), 513–520.
- Johnson, 1998. *Applied Multivariate Methods for Data Analysis*. Duxbury Press, New York, NY.
- Konda Naganathan, G., 2011. *Development and Evaluation of Spectral Imaging Systems and Algorithms for Beef Tenderness Grading*. Dissertation, University of Nebraska-Lincoln.
- Konda Naganathan, G., Grimes, L.M., Subbiah, J., Calkins, C.R., Samal, A., Meyer, G.E., 2008a. Partial least squares analysis of near-infrared hyperspectral images for beef tenderness prediction. *Sens. Instrum. Food Qual. Saf.* 2 (3), 178–188.
- Konda Naganathan, G., Grimes, L.M., Subbiah, J., Calkins, C.R., Samal, A., Meyer, G.E., 2008b. Visible/near-infrared hyperspectral imaging for beef tenderness prediction. *Comput. Electron. Agric.* 64 (2), 225–233.
- Laws, K., 1980. *Textured Image Segmentation*. Dissertation, University of Southern California.
- Li, J., Tan, J., Martz, F.A., Heymann, H., 1999. Image texture features as indicators of beef tenderness. *Meat Sci.* 53 (1), 17–22.
- Li, J., Tan, J., Shatadal, P., 2001. Classification of tough and tender beef by image texture analysis. *Meat Sci.* 57 (4), 341–346.
- Lorenzen, C.L., Hale, D.S., Griffin, D.B., Savell, J.W., Belk, K.E., Frederick, T.L., Miller, M.F., Montgomery, T.H., Smith, G.C., 1993. National Beef Quality Audit: Survey of producer-related defects and carcass quality and quantity attributes. *J. Anim. Sci.* 71 (6), 1495–1502.
- Lorenzen, C., Belk, K., Calkins, C., Miller, R., Morgan, B., O'Connor M., Subbiah, J., 2009. *Validation of Tenderness Prediction Instruments*. National Cattlemen's Beef Association Project Summary.
- Manjunath, B.S., Ma, W.Y., 1996. Texture features for browsing and retrieval of image data. *IEEE Trans. Pattern Anal. Mach. Intell.* 18 (8), 837–842.
- McKenna, D.R., Roebert, D.L., Bates, P.K., Schmidt, T.B., Hale, D.S., Griffin, D.B., Savell, J.W., Brooks, J.C., Morgan, J.B., Montgomery, T.H., Belk, K.E., Smith, G.C., 2002. National Beef Quality Audit-2000: Survey of targeted cattle and carcass characteristics related to quality, quantity, and value of fed steers and heifers. *J. Anim. Sci.* 80 (5), 1212–1222.
- Morgan, J.B., Savell, J.W., Hale, D.S., Miller, R.K., Griffin, D.B., Cross, H.R., Shackelford, S.D., 1991. National beef tenderness survey. *J. Anim. Sci.* 69 (8), 3274–3283.
- Ojala, T., Pietikänen, M., Harwood, D., 1996. A comparative study of texture measures with classification based on feature distributions. *Pattern Recogn.* 29, 51–59.
- Shackelford, S.D., Wheeler, T.L., Koohmaraie, M., 1999. Tenderness classification of beef: II. Design and analysis of a system to measure beef longissimus shear force under commercial processing conditions. *J. Anim. Sci.* 77 (6), 1474–1481.
- Subbiah, J., 2004. *Nondestructive Evaluation of Beef Palatability*. Dissertation, Oklahoma State University.
- Subbiah, J., Calkins, C.R., Samal, A., 2012. *System and Method for Analyzing Material Properties Using Hyperspectral Imaging*. United States Patent (US 8280144B2).
- Subbiah, J., Calkins, C.R., Samal, A., Konda Naganathan, G., 2014. *System and Method for Analyzing Properties of Meat Using Multispectral Imaging*. United States Patent (US 8774469B2).
- USDA, 1997. *United States Standards for Grades of Carcass Beef*. <http://www.ams.usda.gov/AMSV1.0/getfile?dDocName=STELDEV3002979> (accessed October 15, 2014).
- Wu, J., Peng, Y., Li, Y., Wang, W., Chen, J., Dhakal, S., 2012. Prediction of beef quality attributes using VIS/NIR hyperspectral scattering imaging technique. *J. Food Eng.* 109 (2), 267–273.
- Xiong, Z., Sun, D., Zeng, X., Xie, A., 2012. Recent developments of hyperspectral imaging systems and their applications in detecting quality attributes of red meats: A review. *J. Food Eng.* 132, 1–13.